JOURNAL OF IRON AND STEEL RESEARCH, INTERNATIONAL. 2016, 23(4): 350-356

Strengthening Mechanisms for Ti- and Nb-Ti-micro-alloyed High-strength Steels

Chuan-feng MENG[1,2], Yi-de WANG[1,2], Ying-hui WEI[1], Bin-qing SHI[2], Tian-xie CUI[2], Yu-tian WANG[2]

(1. School of Materials Science and Engineering, Taiyuan University of Technology, Taiyuan 030024, Shanxi, China; 2. Technology Center, Taiyuan Iron & Steel (Group) Co., Ltd., Taiyuan 030003, Shanxi, China)

Abstract: The strengthening mechanisms of hot-rolled steels micro-alloyed with Ti (ST-TQ500) and Nb-Ti (NT-TQ500) were investigated by examining the microstructures of steels using optical microscope (OM), scanning electron microscope (SEM) and transmission electron microscope (TEM). The results revealed almost no differences in the solute solution strengthening and fine-grained strengthening of the two steels, whereas the contributions of precipitation strengthening and dislocation strengthening were different for ST-TQ500 and NT-TQ500. The measured precipitation strengthening effect of ST-TQ500 was 88 MPa higher than that of NT-TQ500; this difference was primarily attributed to the stronger precipitation effect of the Ti-containing nanoscale particles. The dislocation strengthening effect of ST-TQ500 was approximately 80 MPa lower than that of NT-TQ500. This is thought to be related to differences in deformation behavior during the finishing rolling stage; the inhibition of dynamic recrystallization from Nb in NT-TQ500 (Nb-Ti) may lead to higher density of dislocations in the microstructure.

Key words: micro-alloying; titanium; niobium; high-strength steel; strengthening mechanism

The strengthening of steel has become important in the automotive industry, construction machinery industry, and other industries because it can reduce the mass of equipment to save energy and reduce emissions[1-4]. Micro-alloying[1-4] is the addition of trace elements (such as Nb, Ti and V) to traditional C-Mn steels or low-alloy steels. In this manner, micro-alloyed elements combined with the thermal mechanical control process (TMCP) technology can control the precipitation behavior of micro-alloyed steels. For example, grain refinement and precipitation strengthening can be used to control the size, morphology, and distribution of carbide and nitride at different temperatures and to improve the strength of steel without loss of toughness or formability.

Previous studies have shown that the strengthening effect is obvious when two or more types of micro-alloyed elements (e.g., Nb-Ti and Nb-V) are added to steels[1-4]. At present, Nb-Ti-micro-alloyed steel is commonly used in construction machinery[5-8]. However, steel production costs are increasing significantly with the rising prices of ore and raw materials. Nb, V, and Ti are the three most commonly used micro-alloying elements. Among these three elements, Ti is the least commonly used; thus, the production of high-strength steels micro-alloyed with only Ti has recently attracted more attention from researchers and producers[5-8]. To date, high-strength steels micro-alloyed with Ti at levels of 450—650 MPa have been produced via compact strip production (CSP)[5-7]. However, there are lack of systematic studies on the Ti-micro-alloyed steels using traditional thick-slab production processes, particularly studies on the strengthening mechanisms of Ti-micro-alloyed high-strength steel. Consequently, this study focused on the strengthening mechanism of Ti-micro-alloyed high-strength steel produced by

Foundation Item: Item Sponsored by National Natural Science Foundation of China (51374151); Foundation for Key Program of Shanxi Province of China (20111101053); Foundation for Major Coal Base New Materials Program of Shanxi Province of China (MC2014-02)

Biography: Chuan-feng MENG, Doctor Candidate, Senior Engineer; **E-mail**: mengcf@tisco.com.cn; **Received Date**: April 17, 2015

Corresponding Author: Ying-hui WEI, Doctor, Professor; **E-mail**: weiyinghui@tyut.edu.cn

the traditional "thick slab + hot rolling" hot-strip process. The properties of Ti-micro-alloyed high-strength steel were compared with those of Nb-Ti-micro-alloyed high-strength steel.

1 Experimental

1.1 Chemical composition and production process

The yield strength level in the two experimental alloys was 500 MPa. The steel micro-alloyed with Ti only was labeled ST-TQ500, and the steel micro-alloyed with Nb-Ti was labeled NT-TQ500. The corresponding chemical compositions are listed in Table 1.

The production route was as follows: hot metal pretreatment→smelting→argon treatment→LF processing→continuous casting→heating→descaling→rough rolling→finish rolling→cooling→coiling. The plate thickness was set to 12 mm. Both ST-TQ500 and NT-TQ500 were processed by the following rolling parameters: finish rolling temperatures of 850—900 ℃ and coiling temperatures of 570—590 ℃.

Table 1 Chemical compositions of the ST-TQ500 and NT-TQ500 steels mass%

Material	C	Si	Mn	P	S	Nb	Ti	Al	N
ST-TQ500	0.071	0.07	1.68	0.01	0.005	0	0.08	0.04	0.0040
NT-TQ500	0.070	0.07	1.71	0.01	0.005	0.04	0.04	0.04	0.0045

1.2 Microstructure and mechanical testing

Tensile specimens were prepared with rectangular cross-section dimensions of 12.5 mm×56.5 mm and were tested at room temperature under a strain rate of 1×10^{-4} s^{-1}. Samples for toughness testing were machined into standard Charpy V-notch specimens with dimensions of 10 mm×10 mm×55 mm. The testing temperature was set as −20 ℃.

Microstructural observation was performed on the longitudinal sections of the samples taken from the tails of coils using optical microscopy (OM), scanning electron microscopy (SEM), and transmission electron microscopy (TEM). The microstructures of samples cut from the 1/2 and 1/4 surfaces of the cast billet were also examined. Samples for TEM with diameters of 3 mm were prepared as follows: the samples were initially abraded to thicknesses of 40 μm; thin films were then prepared by electropolishing with a 5 vol. % perchloric acid-glacial acetic acid solution. TEM was performed using a JEM-2100 microscope.

2 Results and Discussion

2.1 Microstructures

2.1.1 Optical microstructures

Figs. 1(a) and 1(b) show the optical micrographs of the 1/4 longitudinal surfaces of NT-TQ500 and ST-TQ500, respectively. The microstructures were mainly composed of quasi-polygonal ferrite with anomalies in the grain boundaries, obviously different from typical polygonal ferrite, which exhibits smooth and straight grain boundaries. Small amounts of carbides were observed in the grain interiors and boundaries of NT-TQ500 and ST-TQ500. The mean grain size of ferrite in NT-TQ500 was measured to be 3.8 μm, close to that of ST-TQ500 (3.9 μm).

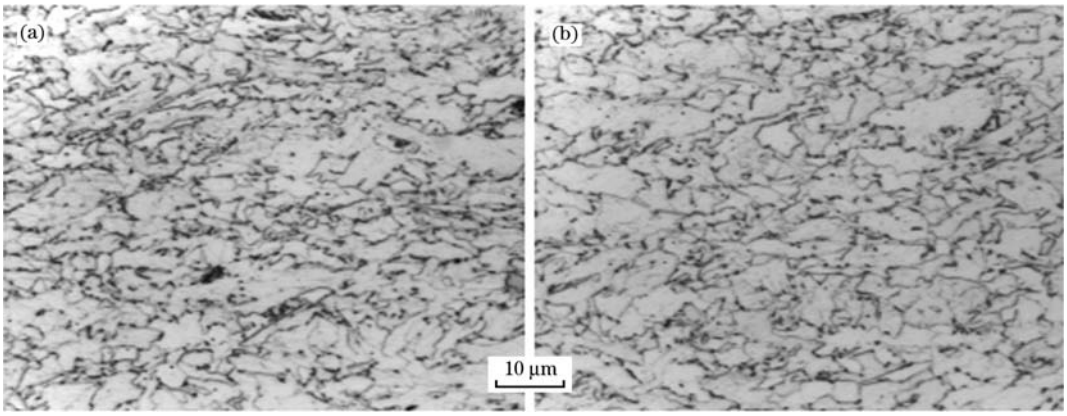

Fig. 1 Optical micrographs of the NT-TQ500 (a) and ST-TQ500 (b) samples

2.1.2 Submicroscale precipitates

To further analyze the differences between the carbides of NT-TQ500 and ST-TQ500, energy dispersive spectrometer (EDS) was used to compare

the chemical compositions of the two steels. The arrows in Figs. 2(a) and 2(b) indicate the typical appearances of the second phases on the submicron scale; the corresponding EDS spectra shows that these phases correspond to carbides/nitrides containing Nb and Ti. Peaks corresponding to nitrogen were not detected in the EDS spectra, which is attributed to a discrepancy in the collecting signals of the electron beam, particularly when the nitrogen composition is low in the second phases[9].

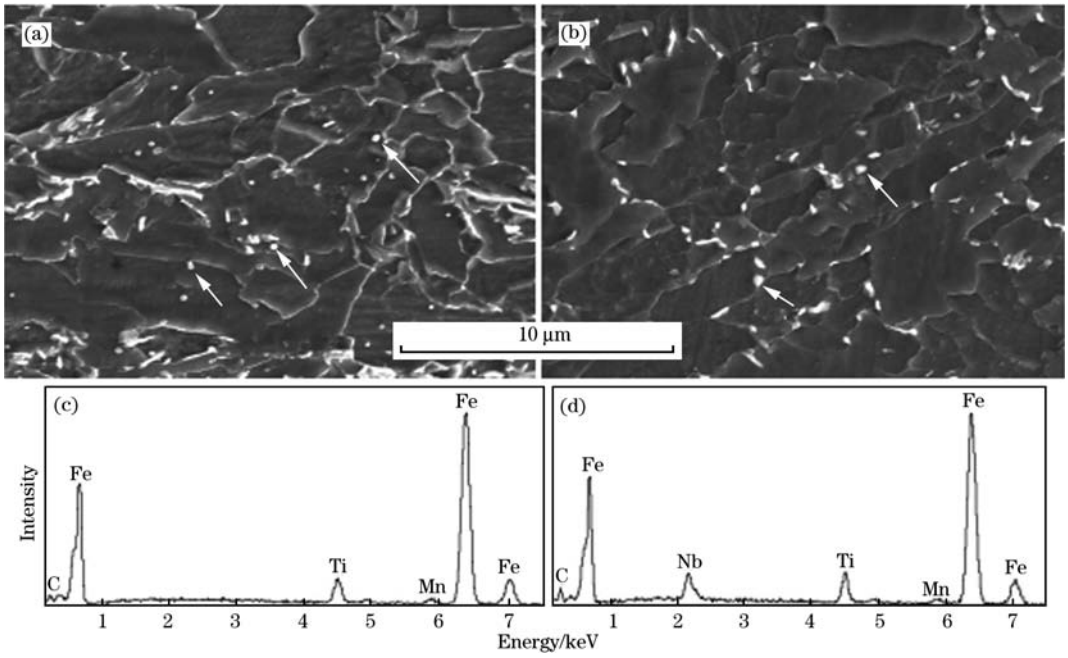

Fig. 2 SEM images of NT-TQ500 (a) and ST-TQ500 (b) and EDS results of second-phase particles of NT-TQ500 (c) and ST-TQ500 (d)

The second phases of ST-TQ500 were mainly distributed at the grain boundaries, which were more homogeneous than those of NT-TQ500. The dimension of second phases for ST-TQ500 (0.2—0.5 μm) was a little lower than that for NT-TQ500.

2.1.3 Nanoscale precipitates in the grain interiors

In addition to the submicron-sized second phases, nanoscale precipitates were observed in the grain interiors. The TEM images in Figs. 3(a) and 3(b) show spherical or ellipsoidal precipitates in NT-TQ500; these are typical of Nb(CN) with an FCC structure[9]. The average size of the nanoscale precipitates was calculated to be 19.3 nm, and the volume fraction was determined to be 3.1 vol.% using Image-Pro plus software.

Figs. 4(a) and 4(b) show the TEM images of the precipitates in ST-TQ500. As shown in the rectangular region in Fig. 4(a), a large amount of nanoscale-second phases were uniformly distributed in the grain interiors, which are more clearly shown

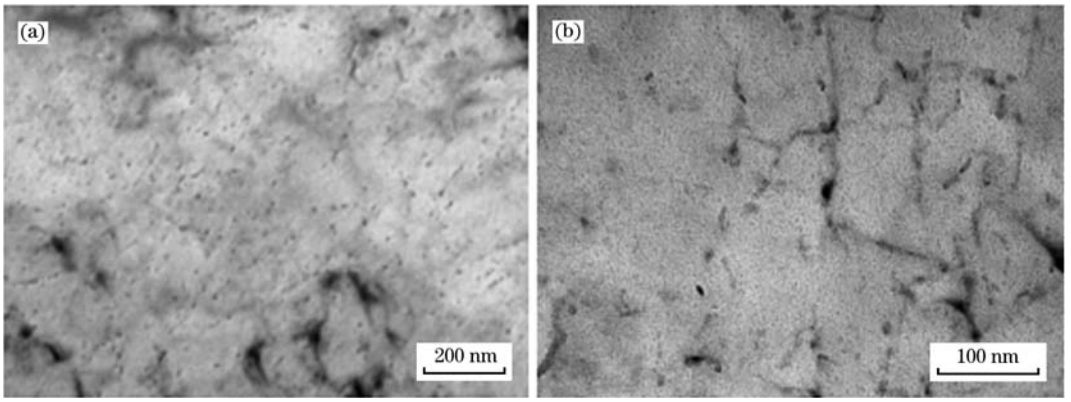

Fig. 3 TEM images of nanoscale precipitates in the grain interiors of NT-TQ500

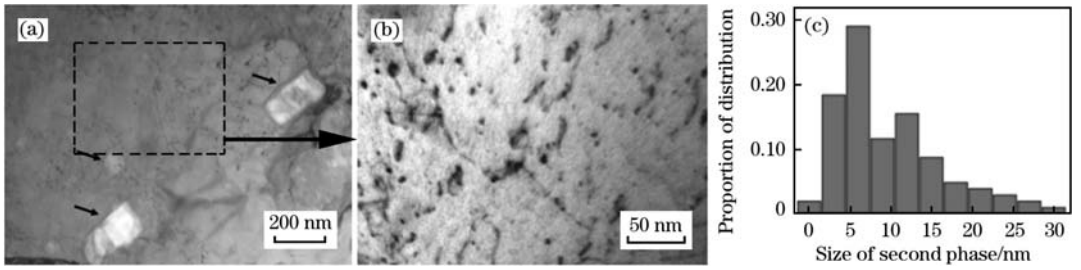

Fig. 4 TEM images of submicron-scale precipitates (a) and nanoscale precipitates in the grain interior of ST-TQ500 (b) and size distribution of the precipitates (c)

in the magnified image in Fig. 4(b). Because of the small particle size, their composition could not be measured quantitatively by EDS, as reported previously[9]. The nanoscale particles were globular in shape with size below 10 nm. Based on their shapes, sizes, and distribution, these particles were speculated to be TiC[9]. Fig. 4(c) shows the size distribution of the nanoscale carbides. The average size and corresponding volume fraction were 12.5 nm and 6.8 vol.%, respectively. Particles with size smaller than 10 nm accounted for approximately 58% of these particles.

Diamond-shaped particles with dimension of approximately 0.2 μm (indicated by the black arrows in Fig. 4(a)), characteristic of the TiN phase, were also observed in the grain interiors. The majority of the TiN particles were submicron scale, and few microscale TiN particles were found in ST-TQ500. Consequently, the microstructures of the 1/4 and 1/2 surfaces of the cast billet of ST-TQ500 were examined (Fig. 5). Only several microscale TiN particles, which were likely precipitated from liquid, were detected in the 1/2 surface.

According to the equation proposed by Turk-

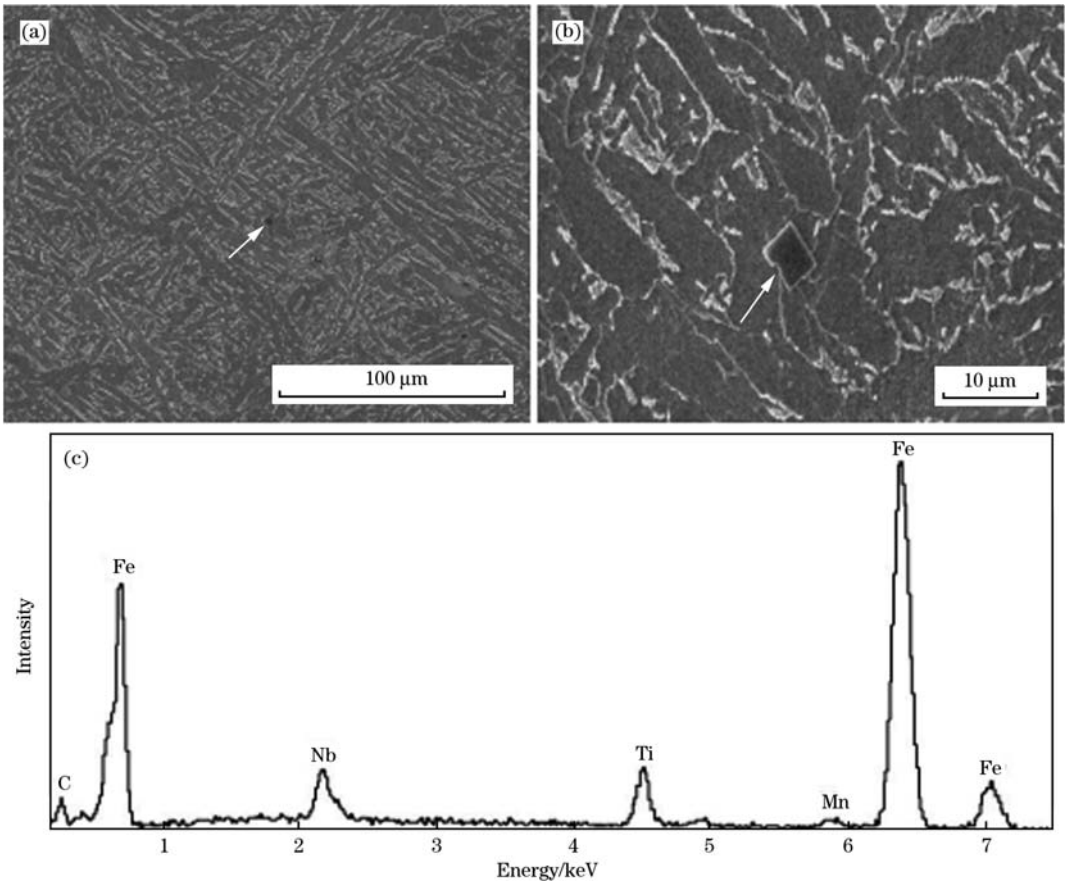

Fig. 5 Typical microscale TiN particle (a), magnified image (b) and corresponding EDS results (c) on the 1/2 surface of the ST-TQ500 cast billet

dogan[10], $\log[Ti][N]=6.4-17040/T$, the solution temperature T of TiN in liquid was calculated to be 1226 ℃ (for mass percentages of Ti ([Ti]) and N ([N]) of 0.08 mass% and 0.004 mass%, respectively). Thus, the majority of submicron-scale TiN particles should precipitate below the solidus temperature. This is because of the low nitrogen content (about 40 ppm) and appropriate secondary cooling technique in the continuous casting process. These submicron-scale TiN particles effectively inhibit grain growth and cause Ti to remain in the matrix, contributing to the precipitation of Ti-bearing nanoscale particles.

2.2 Strengthening mechanisms of Ti- and Ti-Nb-micro-alloyed high-strength steels

The strengthening mechanisms in micro-alloyed ferrite high-strength steels mainly include solute solution strengthening, dislocation strengthening, fine grain strengthening and precipitation strengthening[6,9]. Table 2 shows that the mechanical properties of ST-TQ500, such as strength, plasticity, and toughness, were close to those of NT-TQ500. In the next section, the strengthening mechanisms for ST-TQ500 and NT-TQ500 were compared quantitatively.

2.2.1 *Solute solution strengthening*

According to previous study[9], the resistance of lattice P-N stress in the matrix of the low-carbon steels is given as follows: $\Delta\sigma_0=48$ MPa.

Many studies have confirmed that the increase in yield strength in dilute solute solution $\Delta\sigma_s$ is generally caused by solute solution, as described by the following formula[11]:

$$\Delta\sigma_s=37w_{[Mn]}+83w_{[Si]}+59w_{[Al]}+38w_{[Cu]}+11w_{[Mo]}+33w_{[Ni]}-30w_{[Cr]}+680w_{[P]}+2\,918w_{[N]} \quad (1)$$

where, $w_{[M]}$ represents the mass percent of solute solution elements (M=Mn, Si, …, N). The contribution of solute solution strengthening was evaluated to be 65.7 and 64.3 MPa, representing 10.9% and 10.7% of the overall yield strength, for NT-TQ500 and ST-TQ500, respectively.

2.2.2 *Fine grain strengthening*

The effect of fine grain strengthening is described by the Hall-Petch equation as follows[11]:

$$\Delta\sigma_g=k_y\times d^{-1/2} \quad (2)$$

where, $\Delta\sigma_g$ is quantity of fine grain strengthening; k_y is the coefficient in the equation; and d is the average ferrite grain size. For large-angle grain boundaries, k_y is 15.1—18.1 MPa·mm$^{1/2}$[11]. Zhou et al.[11] selected 16.5 MPa·mm$^{1/2}$ and Wang[9] chose 16.2 MPa·mm$^{1/2}$ in their studies. The average value of 16.35 MPa·mm$^{1/2}$ was used in this study. The effect of fine grain strengthening was evaluated to be 265.2 and 263.6 MPa, representing 44.1% and 44.2% of the overall yield strength, for NT-TQ500 and ST-TQ500, respectively. In other words, the fine grain strengthening effect for NT-TQ500 is close to that for ST-TQ500; the difference is only 1.6 MPa.

2.2.3 *Precipitation strengthening*

The images in Figs. 6(a) and 6(b) show the interactions between precipitates and dislocations for NT-TQ500 and ST-TQ500, respectively. Bending dis-

Table 2 Mechanical properties of ST-TQ500 and NT-TQ500

Steel	Thickness/mm	R_{eL}/MPa	R_m/MPa	A/%	A_{kv}(−20 ℃)/J
ST-TQ500	12	601	685	21.0	123/135/138
NT-TQ500	12	596	674	21.5	168/180/159

Note: R_{eL}—Yield strength; R_m—Tensile strength; A—Elongation-to-failure; A_{kv}(−20 ℃)—Charpy impact energy at −20 ℃.

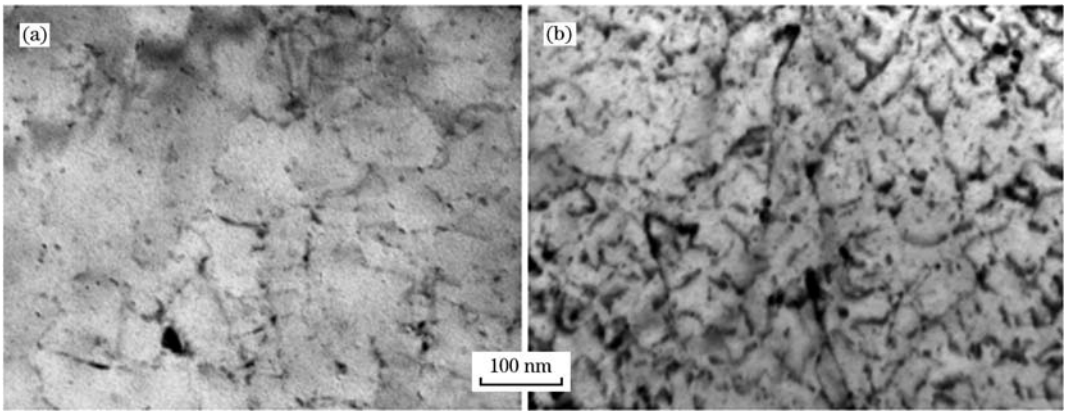

Fig. 6 Typical TEM images showing the interaction between precipitates and dislocations in NT-TQ500 (a) and ST-TQ500 (b)

location joints and dislocation lines, caused by pinning of the second phases, are observed. These features are typical of the so-called "passing-by" mechanism between the second phases and dislocations.

The Orowan strengthening mechanism is described as follows[12]:

$$\Delta\sigma_p = 8.995 \times 10^3 \times f^{1/2}/d \times \ln(2.417d) \quad (3)$$

where, $\Delta\sigma_p$ is the quantity of precipitation strengthening, MPa; f is the volume fraction, vol. %; and d is average diameter of the second phases, mm.

Table 3 lists the effect of precipitation strengthening evaluated by the Orowan mechanism. The size and volume fraction of precipitates were calculated using Image-Pro plus software[13]. The effect of precipitation strengthening accounted for 32.9% and 18.4% of the overall yield strength in ST-TQ500 and NT-TQ500, respectively. The calculated results are in good agreement with the microstructural observations, which reveals a higher volume fraction of nanoscale precipitates in ST-TQ500 than in NT-TQ500.

Table 3 Comparison of precipitation strengthening in NT-TQ500 and ST-TQ500

	Brand	NT-TQ500	ST-TQ500
Intergranular nano precipitates	Species	(NbTi)(CN)	TiC
	Structure	FCC	FCC
	Average volume fraction	3.1%	6.8%
	Average size	19.3 nm	12.5 nm
Precipitation strengthening		110 MPa	198.2 MPa

2.2.4 *Dislocation strengthening*

Dislocation strengthening is another important strengthening mechanism in micro-alloyed ferrite steel[2,9,11]. Dislocation strengthening results from the elastic interaction between dense dislocations formed because of deformation during the hot-rolling process. This interaction enhances the resistance of moving dislocations and consequently strengthens the steel.

Fig. 7 shows the typical dislocation configurations of NT-TQ500 and ST-TQ500. Dense bending and

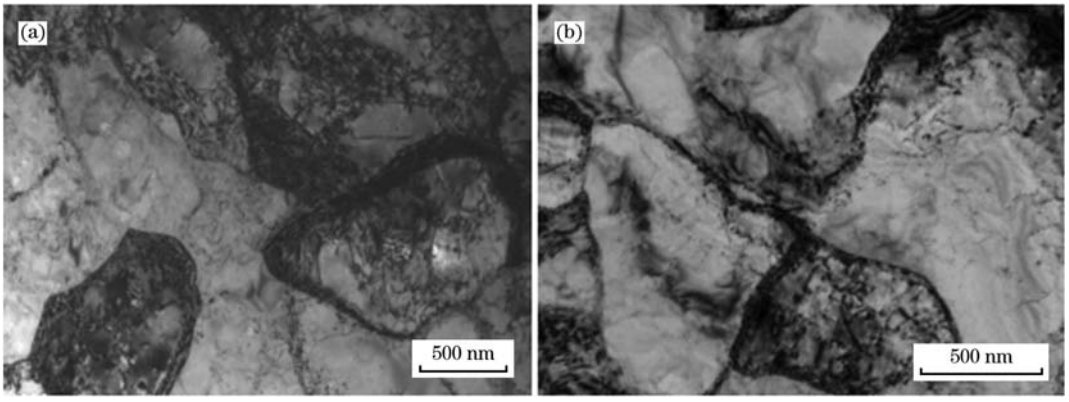

Fig. 7 Typical dislocation configuration morphologies of NT-TQ500 (a) and ST-TQ500 (b)

tangled dislocation lines were observed in the grains of NT-TQ500. High fractions of nanoscale precipitates were dispersed near the bending dislocations or around dislocation nodes. Complete-dislocation cellular structures formed in the region localized with intensive dislocations. Fig. 7(b) shows the typical dislocation structures of ST-TQ500; its dislocation density is lower than that of NT-TQ500. Moreover, regularly arranged cellular structures with sizes of 0.7—2.0 μm were formed.

Based on the original theory of work hardening, the strengthening mechanism of cellular substructure[12], that slipping length is associated with increased deformation[12]. In particular, the dislocation length became shorter to freely expand forward, as the K-R source. This mechanism is in good agreement with previous results[12], which reveales a linear relationship between the true stress and the reciprocal value of average free dislocation length. It should be noted that these studies were based on single-crystal samples and the results are not applicable to the polycrystalline materials studied herein. Because of the lack of relevant data, the strengthening mechanism could not be quantitatively measured in this study. Moreover, dislocations were nonuniformly distributed in NT-TQ500 and ST-TQ500 (Fig. 7). Consequently, it is difficult to quantitatively measure the contribution of dislocation interaction, particularly in regions with high densities of dislocations.

Because of limited contributions of texture and other factors to strength, the dislocation strengthe-

ning $\Delta\sigma_d$ of NT-TQ500 and ST-TQ500 can be calculated as follows:

$$\Delta\sigma_d = \sigma_{YS} - \Delta\sigma_0 - \Delta\sigma_s - \Delta\sigma_g - \Delta\sigma_p \quad (4)$$

where, σ_{YS} is the tested yield strength. $\Delta\sigma_d$ was calculated to be 26.9 and 107.1 MPa, representing 4.5% and 17.9% of the overall yield strength, for ST-TQ500 and NT-TQ500, respectively.

This calculated result is reasonable in comparison with the values reported in the literatures[14,15]. The contribution of dislocation strengthening was calculated to be 46.1 MPa for a dislocation density of 2.8×10^{13} m/m^3 in the ZJ330 plate[14]. In addition, the difference in yield strength was as high as 100 MPa between the same batch of Q690D plates[15], which was suggested to be related to the contribution of dislocations. The differences in the dislocation strengthening between NT-TQ500 and ST-TQ500 are discussed below.

The dislocation density in hot-rolled strips is mainly associated with accumulative deformation during the hot-rolling process. In general, the larger the rolling reduction and the lower the finishing temperature, the greater the contribution of dislocation strengthening to yield strength is. For Nb-bearing NT-TQ500, the dynamic recrystallization temperatures of high-Nb-bearing steels are in the range of 900 to 950 ℃[16]. In contrast, the dynamic recrystallization temperatures for high-Ti-alloyed steel range from 800 to 850 ℃[16]. Moreover, the resistance to deformation of Ti-alloyed steels is much lower than that of high Nb-alloyed steels[16], which is attributed to the stronger resistance to softening in austinite in case of Nb-alloyed alloys. In this study, the finishing rolling temperature ranged from 850 to 900 ℃. In other words, during finish rolling, no recrystallization occurred in NT-TQ500, whereas dynamic recovery or even recrystallization occurred in ST-TQ500. This difference in the rolling process resulted in a higher density of dislocations and a stronger dislocation strengthening effect in ST-TQ500.

3 Conclusions

(1) A high-strength steel micro-alloyed with Ti (ST-TQ500) was developed using a traditional "thick slab + hot rolling" production process. The mechanical properties, including strength, plasticity and toughness, were compared with those of Nb-Ti-micro-alloyed NT-TQ500.

(2) The microstructure ST-TQ500 consisted mainly of polygon ferrite with average grain size of 3.9 μm. The average size and volume fraction of Ti-containing nanoparticles were 12.5 nm and 6.8 vol.%, respectively, and 58% of the nanoparticles were less than 10 nm in size. In terms of strengthening mechanisms, grain refining strengthening, precipitation strengthening, solute solution strengthening, and dislocation strengthening represented 44.1%, 32.9%, 10.9%, and 4.5% of the overall yield strength, respectively.

(3) Comparing the strengthening mechanisms of ST-TQ500, NT-TQ500 revealed similar solute solution strengthening and grain refining strengthening effects. The precipitation strengthening effect of ST-TQ500 was approximately 88 MPa higher than that of NT-TQ500, which was related to a stronger precipitation effect of Ti-containing nanoparticles. The dislocation strengthening effect of ST-TQ500 was 80 MPa lower than that of NT-TQ500 because of the stronger inhibition of austenite recrystallization and higher density of dislocations.

References:

[1] C. E. Armando, C. J. María, P. J. Manuel, J. Iron Steel Res. Int. 18 (2011) Suppl. 1, 148-153.

[2] J. Q. Xu, Y. C. Jia, H. L. Li, S. Sha, S. Jiang, J. Iron Steel Res. Int. 18 (2011) Suppl. 1, 572-575.

[3] P. Sally, R. Andrew, W. Geoff, T. Rachel, J. Iron Steel Res. Int. 18 (2011) Suppl. 1, 208-212.

[4] H. L. Yi, Z. Y. Liu, G. D. Wang, D. Wu, J. Iron Steel Res. Int. 17 (2010) No. 12, 54-58.

[5] L. Q. Xie, X. P. Mao, X. D. Huo, Metallurgical Collections 155 (2005) 1-5.

[6] X. E. Li, Z. Y. Zhao, R. D. Xue, X. Z. Yang, J. X. Xie, Iron and Steel 43 (2008) No. 6, 70-73.

[7] D. M. Wang, F. L. Liu, X. H. Guo, Z. W. Liu, C. Y. Gu, Angang Technology 3 (2008) 21-24.

[8] H. Y. Li, Y. L. Kang, J. J. Wang, P. Zhou, H. S. Tang, Journal of Wuhan University of Science and Technology 33 (2010) 47-52.

[9] R. Z. Wang, H. T. Zhang, Acta Metall. Sin. 43 (2007) 1082-1090.

[10] E. T. Turkdogan, Iron Steelmaker 16 (1989) 61-75.

[11] J. Zhou, Y. L. Kang, X. P. Mao, L. J. Li, Z. Y. Lin, Iron and Steel 41 (2006) 343-350.

[12] F. Brian, Picking, Microstructure and Properties of Steel, Science Press, Beijing, 1999.

[13] X. Y. Yang, G. Xu, J. Yang, K. Zhang, S. Y. Wu, S. P. Zhang, Hot Working Technology 42 (2013) 50-52.

[14] H. Yu, Michanism of Microstructure Refinement and Strengthening of Hot Strip of Low Carbon Steel by CSP Technology, University of Science and Technology Beijing, 2003.

[15] Y. Q. Yang, H. Lei, Q. Gao, Y. L. Li, J. Du, Y. Yuan, Wide and Heavy Plate 19 (2013) 5-10.

[16] H. L. Yi, L. X. Du, G. D. Wang, X. H. Liu, J. Northeast. Univ. Nat. Sci. 28 (2007) 1369-1373.